

GeoTransformer: Enhancing Urban Forecasting with Dependency Retrieval and Geospatial Attention

Yuhao Jia¹, Zile Wu², Shengao Yi³, Yifei Sun⁴,

¹Individual Researcher

yuhaojia98@ucla.edu

²Individual Researcher

³University of Pennsylvania

⁴The Hong Kong University of Science and Technology (Guangzhou)

Abstract

Recent advances in urban forecasting have leveraged high-dimensional spatial data through two primary approaches: graph-based methods that rely on predefined spatial structures and region-based methods that use satellite imagery for local features. Although these methods have laid an important foundation, they struggle to integrate holistic urban information and dynamically model spatial dependencies. To address this gap, we propose GeoTransformer, a framework combining high-dimensional regional embeddings with dynamic spatial modeling. GeoTransformer features two innovations: (1) a dependency retrieval module identifying spatial dependencies to select relevant regions, and (2) a geospatial attention mechanism leveraging global urban information. These components unify structural and global urban information for better predictions. Extensive experiments on GDP and ride-share demand forecasting show that GeoTransformer outperforms baselines, highlighting its effectiveness in advancing urban forecasting tasks.

Introduction

In urban forecasting tasks involving predicting economic indicators and human mobility, classical methods usually rely on low-dimensional numeric data, which includes spatial features, socioeconomic data, human mobility data, and so forth (Li et al. 2022; Roskam and Kunst 2008; DHS et al. 2013; Wang et al. 2023; Moreira-Matias et al. 2013; Papalardo et al. 2013).

Recently, advances in natural language processing (NLP) and deep learning have enabled the use of high-dimensional information to capture the complexities of urban dynamics. Some studies have transformed urban information into high-dimensional representations, either through text embedding (Chen et al. 2022b; Li et al. 2020, 2023), spatial representation learning (Mai, Li, and Lao 2023; Wu et al. 2024b) or by encoding satellite imagery data (Jean et al. 2018; Wang et al. 2024), offering a new urban modeling paradigm by leveraging high-dimensional data to capture complex urban dynamics.

High-dimensional urban forecasting applications can be broadly categorized into two directions. The first utilizes graph-based modeling with spatial feature embeddings, then using Graph Neural Networks (GNNs) or Graph Attention Networks (GATs) for predictions (Feng and Tassiulas 2022;

Zheng et al. 2020; Chen et al. 2022b; Li et al. 2020, 2023). While effective, these methods depend heavily on predefined spatial structures and high-quality spatial data, which limits their flexibility in data-sparse or dynamically changing environments.

Another direction focuses on deriving high-dimensional representations directly from satellite imagery (Jean et al. 2018; Wang et al. 2024). These methods avoid reliance on predefined structures by encoding urban regional information into independent high-dimensional patches. However, these approaches only utilize local information within each patch for prediction and lack the capability to incorporate global urban context (Wang et al. 2024), which is crucial for tasks requiring holistic understanding.

To address these limitations, we propose GeoTransformer, a novel transformer-based (Vaswani et al. 2017) architecture that leverages high-dimensional regional embeddings without requiring predefined spatial structures. GeoTransformer incorporates two key innovations: (1) a dependency retrieval module that infers and integrates urban structural dependencies to retrieve the most relevant regions; and (2) a geospatial attention mechanism, utilizing cross-attention to dynamically capture global urban information, enhanced with spatial proximity and information entropy weighting. These innovations enable GeoTransformer to effectively combine local and global perspectives, offering a robust framework for diverse urban prediction tasks.

Extensive experiments demonstrate that our model significantly outperforms baseline methods in predicting GDP and ride-share demand.

Our main contributions can be summarized as follows:

- We propose GeoTransformer, a novel deep architecture that dynamically models high-dimensional urban representations by integrating global spatial dependencies while eliminating the reliance on predefined spatial structures.
- We introduce two novel modules: a dependency retrieval module that captures urban structures, and a geospatial attention mechanism that prioritizes representations based on spatial proximity and information entropy.
- Experiments demonstrate that our method significantly outperforms baseline models in tasks of GDP and ride-share demand prediction.

Related Work

High-Dimensional Representations for Urban Forecasting

Urban forecasting has increasingly leveraged high-dimensional data to address complex challenges. Traditional approaches often rely on low-dimensional numerical data, such as Point of Interest (POI) data (Li et al. 2022), survey data (Roskam and Kunst 2008; DHS et al. 2013), GPS records (Wang et al. 2023; Moreira-Matias et al. 2013; Papalardo et al. 2013), demographic census, spatial features and so forth, limiting their ability to capture the multifaceted nature of urban dynamics. Recent advances have focused on two primary directions for high-dimensional urban representations.

The first direction employs graph-based methods that embed urban information into representations by constructing predefined graph structures. Graph Attention Networks (GATs) (Zhang, Yu, and Liu 2019) are used to infer POI relationships (Chen et al. 2022b; Li et al. 2020, 2023). Feng and Tassiulas propose an Adaptive Graph Spatial-Temporal Transformer Network to model cross-spatial-temporal correlations. Zheng et al. use a graph multi-attention network to model the impact of the spatio-temporal factors on traffic conditions. Chen et al. propose a spatial-aware attention module based on spatial proximity. Additionally, position embeddings are employed as learnable parameters to provide location information (Xu et al. 2021). These methods rely heavily on predefined spatial structures, such as road networks or adjacency matrices, which limits their applicability in dynamic or data-sparse urban environments.

The second direction focuses on region-based methods that leverage satellite imagery and other high-resolution data to encode urban areas into high-dimensional representations. Tile2Vec (Jean et al. 2018) learns representations from satellite imagery tiles. (Wang et al. 2024) propose a deep hybrid model fusing regional built environment and socio-demographic information into latent representations through multi-task learning. These region-based representation learning methods avoid reliance on predefined graph structures. However, they only leverage local information patches for prediction (Wang et al. 2024) and struggle to incorporate global urban context or dynamically model spatial dependencies. Additionally, region-based representations face variability in effectiveness due to encoding uncertainty, which remains unaddressed. However, information entropy has been shown to evaluate the effectiveness of high-dimensional data (Wu et al. 2024a) and has been used for weighting (Zhu, Tian, and Yan 2020). It offers a method to mitigate these disparities among region-based urban representations, presenting a promising yet underexplored solution.

Urban Spatial Dependency Modeling

Spatial dependency provides key urban structural insights. It has traditionally been addressed through two main approaches for low-dimensional numerical data: feature engineering methods, such as k-nearest neighbors (KNN), and spatial statistical techniques, including spatial error regres-

sion, spatial lag models (Anselin 2013), and geographically weighted regression (GWR) (Fotheringham, Charlton, and Brunsdon 1998).

For high-dimensional representations, GATs employ attention mechanisms to aggregate information from neighboring nodes (Feng and Tassiulas 2022; Zheng et al. 2020; Chen et al. 2022b; Xu et al. 2021). However, region-based high-dimensional urban representations often lack explicit graph-like structures, further complicating their ability to capture spatial dependencies. Data-driven methods like sparse linear layers may provide insights to dynamically capture spatial dependency (Li and Moura 2020), yet their applications on region-based spatial representations remain unexplored.

Therefore, to address these challenges, we propose leveraging a sparse matrix-based dependency retrieval mechanism to dynamically model urban structures and integrating geospatial cross-attention weighted by spatial proximity and information entropy to incorporate both local and global information. These techniques aim to overcome the limitations of predefined graph structures and local-only region-based approaches in existing studies.

Economic and Mobility Indicators Prediction

Gross Domestic Product (GDP) is a critical indicator in urban studies, offering vital insights into the economic health, developmental patterns, and sustainability of cities (Ribeiro et al. 2021; Mahtta et al. 2022; Brilhante and Klaas 2018). Leveraging Nighttime Light (NTL) data to estimate GDP as an economic indicator has become a widely adopted approach (Liu et al. 2021; Sun et al. 2020). There is substantial research indicating a strong association between GDP and urban spatial characteristics (Zhang, He, and Yuan 2020; Zhaoa and Chenb 2023), with numerous studies employing machine learning methods to model and predict regional GDP using structured urban information or urban imagery data (Kopczewska 2022; Chen et al. 2022c). For example, Chen et al. utilize deep learning methods to predict county-level GDP grids. While substantial research has established the relationship between GDP and urban spatial characteristics, the application of high-dimensional urban representations for GDP prediction remains underexplored. Given the critical role of GDP in validating urban prediction models, we selected GDP estimates derived from Nighttime Light (NTL) data as a benchmark for evaluating our approach.

In addition to economic indicators, mobility indicators such as ride-share demand serve as a critical indicator for urban forecasting, and it has significant implications for transportation planning, economic activity, and population behavior (Komanduri et al. 2018; Ma and Hanrahan 2020; Zhang and Zhang 2018). For instance, Shaheen et al. emphasize that ride-share services can influence traffic patterns, reduce private vehicle ownership, and improve accessibility in urban environments. Researchers have developed utilizing deep learning methods to predict ride-share demand from urban spatial information (Mühlematter et al. 2023; Zhao et al. 2022; Tu et al. 2024). Zhao et al. couple graph neural networks (GNNs) with the spatial-temporal influence of the built environment. Zhang and Zhao propose a

Clustering-aided Ensemble Model to improve ridesourcing demand forecasting. Similarly, few studies have explored using high-dimensional urban representations to predict ride-share demand. Given the significance of ride-share demand as a key indicator with strong spatial dependencies, it serves as an ideal benchmark for evaluating the efficacy of our proposed method.

Methodology

GeoTransformer

As illustrated in Figure 1, the whole framework adopts an encoder-decoder structure. The encoder leverages a region-based representation method to process numeric and imagery inputs, representing city regions in a latent space through a mixing operator.

We propose a novel approach GeoTransformer to decode the representations for downstream tasks including GDP and ride-share demand prediction. Our method contains two key innovations: a dependency retrieval module and a geospatial attention module.

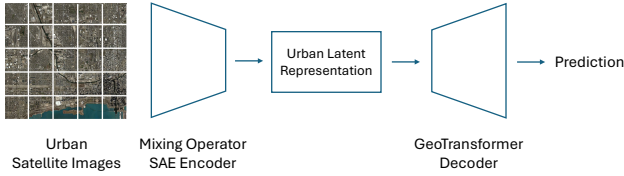


Figure 1: Our urban forecasting framework uses a mixing operator to fuse information into latent representations which are then passed to GeoTransformer for prediction.

As shown in Figure 2, our method adopts a structure akin to the Transformer (Vaswani et al. 2017) decoder. Most relevant regions are retrieved from all urban regions. Then the target and retrieved regions are encoded into representations and then input into the transformer decoder for prediction. The GeoTransformer system \mathcal{G} can be represented as:

$$y_i = \mathcal{G}(z_i, \text{Retrieval}(i, Z)) \quad (1)$$

in which the input includes the latent representation z_i of the target region i and retrieved representations $Z_i = \text{Retrieval}(i, Z)$ from all regions Z , and y_i is the predicted output.

Region-based Urban Representations

To obtain the regional representations, we adopt a mixing operator \mathcal{M} following the work Deep Hybrid Model (Wang et al. 2024), to fuse satellite imagery and sociodemographic information into a high-dimensional latent space, which can be represented as:

$$z_i = \mathcal{M}(x_i, I_i) \quad (2)$$

in which x_i and I_i represent the sociodemographics and satellite imagery inputs, and z_i represents the latent representation of an urban area.

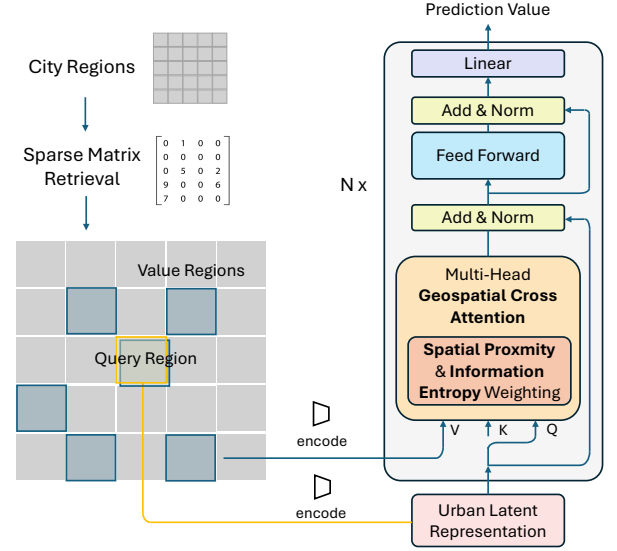


Figure 2: The GeoTransformer framework includes a retrieval module and a geospatial attention module that calculates attention scores between the query region and retrieved value regions.

The supervised autoencoder (SAE) is deployed in this framework to learn the representations through optimizing an autoencoder loss and a sociodemographic supervision loss (Figure 3). Each region of a city is then encoded into a latent representation using the encoder of the trained SAE.

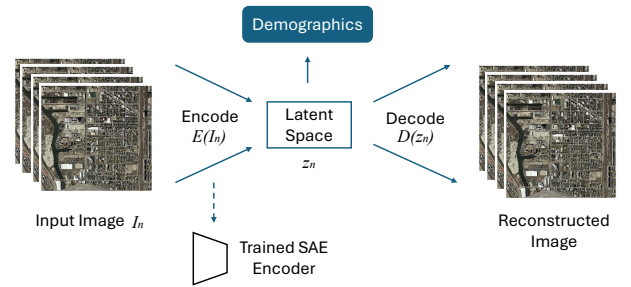


Figure 3: The mixing operator is trained by extracting sociodemographic information and reconstructing the input satellite images from latent space.

Dependency Retrieval Module

To address the challenge of modeling dynamic inter-region interactions for region-based representation methods, we employ a sparse matrix to explicitly represent spatial dependencies. The sparse matrix encodes the influence of one region on another through weights, where only a subset of regions significantly influence the given target region. Building on this, we propose a dependency retrieval mechanism that dynamically identifies the most relevant regions

around the target region as the GeoTransformer model inputs. Specifically, for each target region, the mechanism first identifies the k_1 -nearest neighbors based on spatial proximity. Then, from these k_1 candidates, it selects the top- k_2 regions with the highest weights in the sparse matrix. The retrieval mechanism is defined as:

$$Z_i = \{z_j \mid j \in \arg \text{top}_{k_2}(S[i, \mathcal{N}_{k_1}(i)])\}, \quad (3)$$

where Z_i denotes the set of high-dimensional representations $z_j \in \mathbb{R}^d$ for the k_2 most relevant regions selected from the k_1 -nearest neighbors of the target region i . Here, $\mathcal{N}_{k_1}(i)$ represents the indices of the k_1 -nearest neighbors of region i , identified based on spatial proximity. $S[i, j]$ is the weight from the sparse matrix S , which quantifies the dependency of region i on region j .

The sparse matrix S is constructed using Lasso regression, which enforces sparsity to identify the most important inter-region dependencies. For a given target region i , its high-dimensional representation $z_i \in \mathbb{R}^d$ is treated as the target variable, while the representations of all other regions X serve as input features. The optimization objective for Lasso is defined as:

$$\min_{\beta} \|z_i - X\beta\|_2^2 + \alpha \|\beta\|_1, \quad (4)$$

where $X \in \mathbb{R}^{(n-1) \times d}$ denotes the matrix of feature representations for all other regions except i . The sparse weight vector $\beta \in \mathbb{R}^{n-1}$ captures the influence of other regions on region i , while α is the regularization strength that controls the degree of sparsity in the resulting weights. The Lasso regularization term $\|\beta\|_1$ forces most weights to zero, retaining only the strongest dependencies. The resulting sparse weight vector β is then used to populate the corresponding row $S[i, :]$ in the sparse matrix S .

This dependency retrieval module enables region-based representations to effectively model spatial dependency without predefined urban structure information, providing a foundation for attention computing in the GeoTransformer model.

Geospatial Attention Module

We introduce a geospatial attention mechanism to leverage the global urban information for prediction. As shown in Figure 2, the model first calculates cross-attention between the target and retrieved representations, with the attention scores weighted by spatial proximity and information entropy. The attention calculation is represented as:

$$\text{GeoAtt}(Q, K, V) = (\lambda W_s + (1-\lambda)W_e) \odot \text{softmax}\left(\frac{QK^T}{\sqrt{d_k}}\right)V \quad (5)$$

where the query matrix Q contains the representation of the query region z_i for which the target variable is being predicted, while the value matrix V consists of z_i itself and the retrieved representations as value regions. d_k denotes the dimension of the key vectors. Intuitively, as the similarity between two city regions is not directly related to prediction variables, we set the key matrix K as trainable weights rather than being identical to V . W_s and W_e are the spatial

proximity and information entropy weighting factors respectively. Their relative importance is controlled by a hyperparameter $\lambda \in [0, 1]$.

Spatial Proximity Weighting Our model provides spatial proximity weighting as a way to provide location information. Based on the assumption of Tobler's First Law of Geography (Tobler 1970), we assigned regions closer to the query region with higher weights. We leverage a linear weighting method, scaling the distances within 0 to 1, inversely transforming shorter distances into higher weights:

$$W_{S_j} = 1 - \frac{d_j}{\max(d)} \quad (6)$$

where d_j is the distance to the j^{th} value region, and $\max(d)$ are the maximum distances observed.

Information Entropy Weighting As a way to evaluate the effectiveness of high-dimensional data, we assign higher weights for representations with higher information entropy. Regions with higher entropy are believed to contain richer and more complex urban information, thereby playing a more significant role in prediction. The calculation can be presented as:

$$W_{E_j} = \frac{H_j}{\max(H_1, H_2, \dots, H_n)} \quad (7)$$

where H_i is the Shannon entropy of the latent representation z_i , and $\max(H_1, H_2, \dots, H_n)$ is the maximum entropy across retrieved tiles. Since the latent representation is a high-dimensional vector z_i , the entropy H_i for each individual latent representation can be represented as:

$$H_j = - \sum_{i=1}^d p_{ji} \log(p_{ji}) \quad (8)$$

$$\text{where } p_{ij} = \frac{e^{z_{ij}}}{\sum_{k=1}^d e^{z_{ik}}} \quad (9)$$

Here, z_{ji} is the value of the j -th feature for latent representation z_i , and p_{ij} is the normalized probability.

Adhering to the established multi-head attention mechanism (Vaswani et al. 2017), our model employs multiple attention heads to capture various spatial relationships concurrently. The calculation can be represented as:

$$\text{MultiHead}(Q, K, V) = \text{Concat}(\text{head}_1, \dots, \text{head}_h)W^O \quad (10)$$

$$\text{where } \text{head}_i = \text{GeoAtt}(QW_i^Q, KW_i^K, VW_i^V) \quad (11)$$

where W_i^Q , W_i^K , W_i^V and W^O are the projection matrices. The amount of heads and layers of the decoder module is also adaptive. At last, the outputs of the decoder layers are passed through a fully connected linear layer.

The GeoTransformer framework is designed to overcome limitations in region-based urban representation methods, capturing spatial dependency dynamically and leveraging global urban information for prediction. It is also adaptable to various urban prediction tasks due to the flexibility of the output layers. Overall, our GeoTransformer represents a novel approach to geospatial analysis and urban planning applications.

Panel 1 Deep Hybrid Model Framework (Latent Representations + Regression)	
Model 1: DHM (linear)	representation input (4096 dim), Linear Regression
Model 2: DHM (polynomial)	representation input (reduced dim from 4096 to 128 using PCA), Polynomial Regression (poly degree = 2, l_2 regularization $\lambda = 0.5$)
Panel 2 Latent Representations + Graph Attention Networks	
Model 3: GAT (grid)	representation input (4096 dim), layers = 4
Model 4: GAT (sparse)	representation input (4096 dim), layers = 4, retrieval size = 81
Panel 3 Latent Representations + GeoTransformer (Ours)	
Model 5: GeoTransformer	representation input (4096 dim), heads = 16, layers = 4, KNN=121, retrieval size = 81

Table 1: Training settings of baselines and GeoTransformer models.

GDP and Ride-share Demand Modeling

For the GDP modeling, we use the Global 1km×1km gridded revised data (Chen et al. 2022a) which is based on night-time light data from DMSP/OLS and NPP/VIIRS sensors. The data is calibrated across different years and sensors to produce a consistent high-resolution dataset. A regression model is constructed by linking night-time light intensity, population density, and other auxiliary variables with actual GDP. the gridded real GDP can be calculated using:

$$RGY_{ij,t}^* = \begin{cases} \frac{RGY_{ij,t+1}^*}{1+gy_{ij,t}}, & \text{if } DN_{ij,t} \neq 0 \\ 0, & \text{if } DN_{ij,t} = 0 \end{cases} \quad (12)$$

where $RGY_{ij,t}^*$ denotes the j^{th} grid in the i^{th} country’s real GDP in the period of t based on the revised real growth rate. The calculations are based on the hypothesis that there is no GDP when the DN value is zero. The original GDP data, gridded at 1km×1km resolution, is resampled using bilinear interpolation.

For the ride-share demand modeling, we utilize taxi trip data from Chicago that is constant with the time frame of the remote sensing imagery. Focusing on the pickup locations to represent ride-share demand, we aggregate the demand for each census tract by calculating the total number of pickups within each tract. Subsequently, we apply area-weighted averaging to estimate the ride-share demand corresponding to each imagery. The area-weighted average ride-share demand \bar{D} for each imagery is calculated as follows:

$$\bar{D} = \frac{\sum_{i=1}^n D_i \cdot A_i}{\sum_{i=1}^n A_i} \quad (13)$$

where D_i is the ride-share demand (number of pickups) in the i -th census tract, A_i is the area of the i -th census tract, and n is the total number of census tracts. This approach allows us to align the spatial resolution of the taxi trip data with the remote sensing imagery, facilitating accurate and effective modeling of ride-share demand.

Experiment

In this section, we provide our method’s experiments in GDP and ride-share demand prediction and compare them with

baseline methods. Ablation experiments are conducted to demonstrate the effectiveness of the dependency retrieval module and two weighting methods in the geospatial attention module.

Experiment Setup

Data Preparation. For the satellite imagery data, we utilized the National Agriculture Imagery Program (NAIP) four-band remote sensing imagery for the Greater Chicago Area, acquired in September 2019. The imagery has a high spatial resolution of 0.6 meters. Using Google Earth Engine, we download the dataset and subsequently divide it into tiles of size 512x512 to facilitate our analysis.

For spatial correspondence between structured and unstructured information, we created a fishnet grid with a cell size of 500m×500m, aligned it with the same geospatial location as the maptile data, and resampled the 1km×1km gridded GDP data to match the fishnet.

For the ride-share demand, we use the Taxi Trips dataset obtained from the City of Chicago. The dataset includes fundamental trip information such as unique ID, pickup and drop-off timestamps, latitude and longitude coordinates, trip miles, fare, and other relevant details. To align the spatial resolution of the taxi trip data with the satellite imagery tiles, we performed a spatial join. This process allows us to calculate the ride-share demand corresponding to each tile, ensuring accurate and effective integration of the two data sources.

In addition to the imagery and ride-share data, we incorporate sociodemographic data from the American Community Survey (ACS) 2015-2019. This dataset provides detailed information at the census tract level, including variables such as median rent, racial composition, median household income, the Gini index, and so on.

Mixing Operator Training. We utilize the VAE component from Stable Diffusion (Rombach et al. 2022) as the initial weights for the mixing operator. To accommodate a 4096-dimensional latent space, linear layers are introduced at both the encoder’s output and the decoder’s input. The decoder reconstructs images using mean absolute error (MAE) as the reconstruction loss. An annealing strategy is

Model	GDP			Ride-share Demand		
	MSE ↓	MAE ↓	R^2	MSE $\times 10^7$ ↓	MAE $\times 10^3$ ↓	R^2
<i>Panel 1 Deep Hybrid Model Framework (Latent Representations + Regression)</i>						
1 DHM (linear)	3.56/3.23	1.84/1.75	0.151/0.142	9.03/7.28	9.36/8.90	0.568/0.601
2 DHM (polynomial)	2.19/3.25	1.17/1.46	0.429/0.118	12.8/19.5	5.05/6.00	0.494/0.335
<i>Panel 2 Latent Representations + Graph Attention Networks</i>						
3 GAT (grid)	0.469/0.726	0.476/0.602	0.866/0.805	7.21/9.51	2.01/2.35	0.750/0.575
4 GAT (sparse)	0.592/0.691	0.547/0.561	0.852/0.812	6.22/5.47	1.66/1.83	0.781/0.794
<i>Panel 3 Latent Representations + GeoTransformer (Ours)</i>						
5 GeoTransformer	0.079/0.216	0.207/0.343	0.964/0.933	0.217/2.94	0.684/1.02	0.920/0.901

Table 2: Predictive performance of baselines and GeoTransformer models. Each entry is represented as training/testing performance.

adopted for the KL divergence loss, gradually increasing its weight ratio. Additionally, the latent space restores sociodemographic information through a feed-forward module, employing mean squared error (MSE) as the loss metric. The training process spans 100 epochs in total. The latent representation for each region is inferred using the encoder part of the mixing operator.

Baselines. We train various baseline models for comparison. As detailed in Table 1, models in Panel 1 utilize the deep hybrid model (DHM) (Wang et al. 2024) framework, directly inputting representations to regression models to predict. Specifically, Model 1 employs a linear regression, and Model 2 utilizes a polynomial regression. Panel 2 presents models that utilize representations as inputs for graph attention networks (GATs). Model 3 forms the graph structure by assigning each region as a node connected to its rook neighbors. Model 4 constructs a graph using the sparse matrix, where each region is a node connected to its top- k relevant neighbors selected by the highest weights in our sparse matrix, with edges weighted accordingly. The number of top- k connections in Model 4 is consistent with the retrieval size in GeoTransformer, while all other hyperparameters for training the baseline models are optimized through a grid search to ensure peak performance on the test set.

GeoTransformer Training. As shown in Table 1 panel 3, we train the GeoTransformer (model 5) with the number of decoder layers set to 4, and the number of attention heads set to 16. The L2 regularization decay weight is optimized at 0.001, while the number of retrieved regions is set to 81. All parameters are grid-searched to ensure the best performance. For both GDP and ride-share demand predictions, mean squared error (MSE) is employed as the loss function. All models are trained on an RTX 4090 GPU running Ubuntu 22.04.

Evaluation Metrics. We employ commonly used statistical metrics that evaluate the accuracy of the predictions, including Mean Squared Error (MSE), Mean Absolute Er-

ror (MAE), and R-squared (R^2). MSE evaluates the average squared differences between predicted and actual values, MAE measures the average absolute differences, and (R^2) assesses the proportion of variance explained by the model.

Evaluation Results

Table 2 summarizes the predictive performance evaluation of baselines and the GeoTransformer model in both GDP and ride-share demand prediction tasks.

GDP Prediction. As shown in Table 2, our GeoTransformer model surpasses every baseline model. For Deep Hybrid Models in panel 1, linear regression performs a little better than polynomial regression, and our model outperforms them by around 80% in R^2 . In Panel 2, the GAT models exhibit similar capabilities for decoding region-based representations to predict GDP, with over 80% in R^2 , while our GeoTransformer still surpasses them by 10% in R^2 .

Ride-share Demand Prediction. The results in Panel 1 of Table 2 show that both Deep Hybrid Models achieve 60% and 33% in R^2 respectively, while GeoTransformer surpasses them over 33 % in R^2 . In panel 2, the GAT model based on our sparse matrix achieves nearly 80% in R^2 , around 22% higher than the one with grid structure. However, our GeoTransformer model still outperforms it by 13% in R^2 on the test set.

Our method significantly outperforms the deep hybrid models relying solely on single-region representations across both prediction tasks, demonstrating the substantial accuracy gains achieved by leveraging global urban information. Notably, GeoTransformer’s retrieval mechanism, which captures urban structural information without relying on predefined urban structures, exhibits clear superiority over GAT models that utilize graph structures built from the same information. This highlights the effectiveness of GeoTransformer in dynamically modeling urban dependencies and extracting meaningful global context for enhanced

Model	MSE↓	MAE↓	R^2
1 Random Regions + No Attention Weighting	3.24/3.84	1.54/1.65	0.061/0.007
2 Retrieved Module + No Attention Weighting	0.618/0.650	0.596/0.708	0.811/0.758
3 Retrieved Module + Spatial Proximity Weighting	0.245/0.418	0.364/0.478	0.906/0.881
4 Retrieved Module + Spatial Proximity & Information Entropy Weighting	0.079/0.216	0.207/0.343	0.964/0.933

Table 3: Ablation experimental results of each GeoTransformer component.

predictive performance.

Qualitative Analysis

To investigate the functionality of the dependency retrieval module, we visualize several top retrieval results for the target region. Figure 4 presents an example of a satellite image of the target region in the northwest area of the Auburn Gresham community and six top relevant regions based on the sparse matrix. The relevant regions span two major urban area types. The first includes functional zones near the target, such as local middle schools, parks, and churches (Region a-d in Figure 4). The second type of area covers transportation hubs within the community, such as railway hub centers and main roads within the community (Region e and f in Figure 4). These results showcase our retrieval module’s ability to capture urban structures within the specific spatial scale using the sparse matrix.

In addition to balancing the inconsistency in the information effectiveness of individual representation samples during the encoding process, we also argue that higher information entropy represents more complex and diverse regions, which is demonstrated by comparing regional representations with high and low information entropy (figure 5).

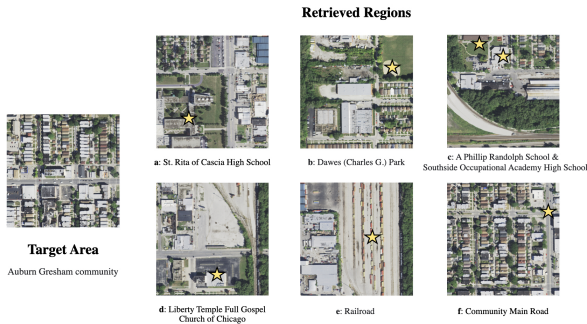


Figure 4: An example of dependency retrieval results.

Ablation Study

To investigate the necessity and effectiveness of each design in GeoTransformer, we conduct ablation experiments for the dependency retrieval module and two weighting methods for the geospatial attention module. The experiment setup and results for GDP prediction are shown in Table 3.

Four models were designed for the ablation study to evaluate the effectiveness of each component in GeoTrans-

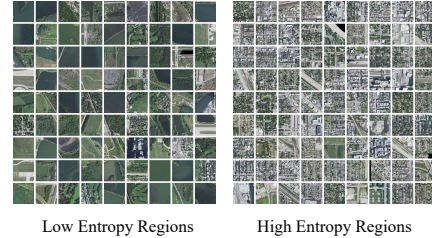


Figure 5: A comparison of high and low information entropy regions.

former. Model 1 uses randomly selected regions without any attention weighting, serving as a baseline to demonstrate the importance of retrieval and attention weighting mechanisms. Model 2 applies the dependency retrieval mechanism on Model 1 to select relevant regions. Model 3 builds upon Model 2 by introducing spatial proximity weighting. Finally, Model 4 represents the complete GeoTransformer design, integrating the dependency retrieval module and both spatial proximity weighting and information entropy weighting to refine the attention mechanism.

The experimental results, presented in Table 3, show a clear and consistent improvement in performance with each added component. Model 1, with random selection, yields an R_2 near zero, indicating a chaotic model, while Model 2 introduces spatial dependencies through the retrieval mechanism, achieving a dramatic leap to over 80% R_2 , demonstrating the effectiveness of the retrieval mechanism in selecting relevant regions. The addition of spatial proximity weighting in Model 3 further enhances accuracy, validating the importance of incorporating spatial relationships into the attention module. Finally, Model 4 achieves the best performance across all metrics, confirming the necessity of applying information entropy weighting.

Conclusion and Discussion

GeoTransformer demonstrates robust capabilities in urban forecasting, establishing a novel paradigm for region-based representation methods without reliance on predefined urban structural information. The experimental results validate the capacity of GeoTransformer, with ablation studies further highlighting the effectiveness of its key components. GeoTransformer still has limitations as it focuses solely on static validation and does not explore time-series tasks. However, the combination of the novel retrieval mechanism and attention-based model lays a strong foundation for future advancements in spatiotemporal forecasting.

References

- Anselin, L. 2013. *Spatial econometrics: methods and models*, volume 4. Springer Science & Business Media.
- Brilhante, O.; and Klaas, J. 2018. Green city concept and a method to measure green city performance over time applied to fifty cities globally: Influence of GDP, population size and energy efficiency. *Sustainability*, 10(6): 2031.
- Chen, J.; Gao, M.; Cheng, S.; Hou, W.; Song, M.; Liu, X.; and Liu, Y. 2022a. Global 1 km \times 1 km gridded revised real gross domestic product and electricity consumption during 1992–2019 based on calibrated nighttime light data. *Scientific Data*, 9(1): 202.
- Chen, Y.; Li, X.; Cong, G.; Long, C.; Bao, Z.; Liu, S.; Gu, W.; and Zhang, F. 2022b. Points-of-Interest Relationship Inference with Spatial-enriched Graph Neural Networks. arXiv:2202.13686.
- Chen, Y.; Wu, G.; Ge, Y.; and Xu, Z. 2022c. Mapping gridded gross domestic product distribution of China using deep learning with multiple geospatial big data. *Ieee Journal of Selected Topics in Applied Earth Observations and Remote Sensing*, 15: 1791–1802.
- DHS, M.; et al. 2013. Demographic and health surveys. *Calverton: Measure DHS*.
- Feng, A.; and Tassioulas, L. 2022. Adaptive graph spatial-temporal transformer network for traffic forecasting. In *Proceedings of the 31st ACM international conference on information & knowledge management*, 3933–3937.
- Fotheringham, A. S.; Charlton, M. E.; and Brunsdon, C. 1998. Geographically weighted regression: a natural evolution of the expansion method for spatial data analysis. *Environment and planning A*, 30(11): 1905–1927.
- Jean, N.; Wang, S.; Samar, A.; Azzari, G.; Lobell, D.; and Ermon, S. 2018. Tile2Vec: Unsupervised representation learning for spatially distributed data. arXiv:1805.02855.
- Komanduri, A.; Wafa, Z.; Proussaloglou, K.; and Jacobs, S. 2018. Assessing the impact of app-based ride share systems in an urban context: Findings from Austin. *Transportation Research Record*, 2672(7): 34–46.
- Kopczewska, K. 2022. Spatial machine learning: new opportunities for regional science. *The Annals of Regional Science*, 68(3): 713–755.
- Li, S.; Zhou, J.; Xu, T.; Liu, H.; Lu, X.; and Xiong, H. 2020. Competitive analysis for points of interest. In *Proceedings of the 26th ACM SIGKDD International Conference on Knowledge Discovery & Data Mining*, 1265–1274. ACM.
- Li, T.; Xin, S.; Xi, Y.; Tarkoma, S.; Hui, P.; and Li, Y. 2022. Predicting multi-level socioeconomic indicators from structural urban imagery. In *Proceedings of the 31st ACM international conference on information & knowledge management*, 3282–3291.
- Li, Y.; Huang, W.; Cong, G.; Wang, H.; and Wang, Z. 2023. Urban region representation learning with open-streetmap building footprints. In *Proceedings of the 29th ACM SIGKDD Conference on Knowledge Discovery and Data Mining*, 1363–1373. ACM.
- Li, Y.; and Moura, J. M. 2020. Forecaster: A graph transformer for forecasting spatial and time-dependent data. In *ECAI 2020*, 1293–1300. IOS Press.
- Liu, H.; He, X.; Bai, Y.; Liu, X.; Wu, Y.; Zhao, Y.; and Yang, H. 2021. Nightlight as a proxy of economic indicators: Fine-grained GDP inference around Chinese mainland via attention-augmented CNN from daytime satellite imagery. *Remote Sensing*, 13(11): 2067.
- Ma, N. F.; and Hanrahan, B. V. 2020. Unpacking sharing in the peer-to-peer economy: The impact of shared needs and backgrounds on ride-sharing. *Proceedings of the ACM on Human-Computer Interaction*, 4(CSCW1): 1–19.
- Mahtta, R.; Fragkias, M.; Güneralp, B.; Mahendra, A.; Reba, M.; Wentz, E. A.; and Seto, K. C. 2022. Urban land expansion: the role of population and economic growth for 300+ cities. *Npj Urban Sustainability*, 2(1): 5.
- Mai, G.; Li, Z.; and Lao, N. 2023. Spatial Representation Learning in GeoAI. In *Handbook of Geospatial Artificial Intelligence*, 99–120. Boca Raton, FL: CRC Press.
- Moreira-Matias, L.; Gama, J.; Ferreira, M.; Mendes-Moreira, J.; and Damas, L. 2013. Predicting taxi–passenger demand using streaming data. *IEEE Transactions on Intelligent Transportation Systems*, 14(3): 1393–1402.
- Mühlematter, D. J.; Wiedemann, N.; Xin, Y.; and Raubal, M. 2023. Spatially-aware car-sharing demand prediction. *arXiv preprint arXiv:2303.14421*.
- Pappalardo, L.; Rinzivillo, S.; Qu, Z.; Pedreschi, D.; and Giannotti, F. 2013. Understanding the patterns of car travel. *The European Physical Journal Special Topics*, 215: 61–73.
- Ribeiro, H. V.; Oehlers, M.; Moreno-Monroy, A. I.; Kropp, J. P.; and Rybski, D. 2021. Association between population distribution and urban GDP scaling. *Plos one*, 16(1): e0245771.
- Rombach, R.; Blattmann, A.; Lorenz, D.; Esser, P.; and Ommer, B. 2022. High-resolution Image Synthesis with Latent Diffusion Models. In *Proceedings of the IEEE/CVF Conference on Computer Vision and Pattern Recognition (CVPR)*, 10684–10695. New Orleans, LA: IEEE.
- Roskam, A.-J. R.; and Kunst, A. E. 2008. The predictive value of different socio-economic indicators for overweight in nine European countries. *Public health nutrition*, 11(12): 1256–1266.
- Shaheen, S.; Chan, N.; Bansal, A.; and Cohen, A. 2015. Shared mobility: Definitions, industry developments, and early understanding. *Transportation Sustainability Research Center, Innovative Mobility Research*.
- Sun, J.; Di, L.; Sun, Z.; Wang, J.; and Wu, Y. 2020. Estimation of GDP using deep learning with NPP-VIIRS imagery and land cover data at the county level in CONUS. *IEEE Journal of Selected Topics in Applied Earth Observations and Remote Sensing*, 13: 1400–1415.
- Tobler, W. R. 1970. A computer movie simulating urban growth in the Detroit region. *Economic geography*, 46(sup1): 234–240.

- Tu, W.; Ye, H.; Mai, K.; Zhou, M.; Jiang, J.; Zhao, T.; Yi, S.; and Li, Q. 2024. Deep online recommendations for connected E-taxis by coupling trajectory mining and reinforcement learning. *International Journal of Geographical Information Science*, 38(2): 216–242.
- Vaswani, A.; Shazeer, N.; Parmar, N.; Uszkoreit, J.; Jones, L.; Gomez, A. N.; Kaiser, L.; and Polosukhin, I. 2017. Attention Is All You Need. *arXiv:1706.03762*.
- Wang, Q.; Wang, S.; Zheng, Y.; Lin, H.; Zhang, X.; Zhao, J.; and Walker, J. 2024. Deep hybrid model with satellite imagery: How to combine demand modeling and computer vision for travel behavior analysis? *Transportation Research Part B: Methodological*, 179: 102869.
- Wang, Z.; Sun, Y.; Lei, Z.; Zhu, X.; and Sun, P. 2023. SST: A Simplified Swin Transformer-based Model for Taxi Destination Prediction based on Existing Trajectory. In *2023 IEEE 26th International Conference on Intelligent Transportation Systems (ITSC)*, 1404–1409.
- Wu, H.; Chen, Y.; Zhu, W.; Cai, Z.; Heidari, A. A.; and Chen, H. 2024a. Feature selection in high-dimensional data: an enhanced RIME optimization with information entropy pruning and DBSCAN clustering. *International Journal of Machine Learning and Cybernetics*, 1–44.
- Wu, N.; Cao, Q.; Wang, Z.; Liu, Z.; Qi, Y.; Zhang, J.; Ni, J.; Yao, X.; Ma, H.; Mu, L.; Ermon, S.; Ganu, T.; Nambi, A.; Lao, N.; and Mai, G. 2024b. TorchSpatial: A Location Encoding Framework and Benchmark for Spatial Representation Learning. *arXiv preprint arXiv:2406.15658*.
- Xu, M.; Dai, W.; Liu, C.; Gao, X.; Lin, W.; Qi, G.-J.; and Xiong, H. 2021. Spatial-Temporal Transformer Networks for Traffic Flow Forecasting. *arXiv:2001.02908*.
- Zhang, C.; Yu, J. J. Q.; and Liu, Y. 2019. Spatial-Temporal Graph Attention Networks: A Deep Learning Approach for Traffic Forecasting. *IEEE Access*, 7: 166246–166256.
- Zhang, J.; He, X.; and Yuan, X.-D. 2020. Research on the relationship between Urban economic development level and urban spatial structure—A case study of two Chinese cities. *PLoS One*, 15(7): e0235858.
- Zhang, X.; and Zhao, X. 2022. Machine learning approach for spatial modeling of ridesourcing demand. *Journal of Transport Geography*, 100(C).
- Zhang, Y.; and Zhang, Y. 2018. Exploring the relationship between ridesharing and public transit use in the United States. *International journal of environmental research and public health*, 15(8): 1763.
- Zhao, T.; Huang, Z.; Tu, W.; He, B.; Cao, R.; Cao, J.; and Li, M. 2022. Coupling graph deep learning and spatial-temporal influence of built environment for short-term bus travel demand prediction. *Computers, Environment and Urban Systems*, 94: 101776.
- Zhaoha, L.; and Chenb, B. 2023. Analysis and Forecast of GDP in Shaoguan City Based on ARIMA Model. *Academic Journal of Business & Management*, 5(21): 117–122.
- Zheng, C.; Fan, X.; Wang, C.; and Qi, J. 2020. GMAN: A Graph Multi-Attention Network for Traffic Prediction. In *Proceedings of the AAAI Conference on Artificial Intelligence*, 1234–1241. Menlo Park, Calif.: AAAI Press.
- Zhu, Y.; Tian, D.; and Yan, F. 2020. Effectiveness of entropy weight method in decision-making. *Mathematical Problems in Engineering*, 2020(1): 3564835.